FIBER BASED SPECTRAL DOMAIN OPTICAL COHERENCE TOMOGRAPHY: MECHANISM AND CLINICAL APPLICATIONS

By

Leo Renyuan Zhang

A Thesis Submitted to the Faculty of the

COLLEGE OF OPTICAL SCIENCES

In Partial Fulfillment of the Requirements

For the Degree of

MASTER OF SCIENCE

IN OPTICAL SCIENCES

THE UNIVERSITY OF ARIZONA

2015

FIBER BASED SPECTRAL DOMAIN OPTICAL COHERENCE TOMOGRAPHY: MECHANISM AND CLINICAL APPLICATIONS

By

Leo Renyuan Zhang

Examination committee:
Dr. Khanh Kieu
Assistant Professor of Optical Sciences, Chairman
Dr. Robert A. Norwood
Professor of Optical Sciences, Committee Member
Dr. Leilei Peng
Assistant Professor of Optical Sciences, Committee Member

Abstract

Optical Coherence Tomography (OCT) is a novel, non-invasive, micrometer-scale-solution tomography, which use coherent light to obtain cross-sectional images of specific samples, such as biological tissue. Spectral Domain Optical Coherence Tomography (SD-OCT) is the second generation of Optical Coherence Tomography. In comparison to the first generation Time Domain Optical Coherence Tomography (TD-OCT), SD-OCT is superior in terms of its capturing speed, signal to noise ratio, and sensitivity. The SD-OCT has been widely used in both clinical and research imaging.

The primary goal of this research is to design and construct a Spectral Domain Optical Coherence Tomography system which consists of a fiber-based imaging system and a line scan CCD-based high-speed spectrometer, and is capable of imaging and analyzing biological tissue at a wavelength of 1040 nm. Additionally, a NI LabVIEW software for controlling, acquiring and signal processing is developed and implemented. An axial resolution of 16.9 micrometer is achieved, and 2-D greyscale images of various samples have been obtained from our SD-OCT system. The device was initially calibrated using a glass coverslip, and then tested on multiple biological samples, including the distal end of a human fingernail, onion peels, and pancreatic tissues. In each of these images, both tissue and cell structures were observed at depths of up to 0.6 millimeter. The A-scan processing time is 8.445 millisecond. Our SD-OCT system demonstrates tremendous potential in becoming a vital imaging tool for clinicians and researchers.

Contents

List of Figures

List of Tables

Chapter 1 Introduction

1.1 Optical Coherence Tomography

Tomography technology has been developed rapidly over the last 50 years. Among most tomography inventions, Computed Tomography (CT) and Magnetic Resonance Imaging (MRI) have already been applied in radiology and medical diagnosis to investigate anatomy and physiology.[1]

Optical Coherence Tomography (OCT) is a relatively new technology which demonstrates better axial resolution (in comparison to other existing tomography technologies). Because of its micrometer resolution and millimeter penetration depth, OCT technology has been applied in biomedical imaging to produce high-resolution cross-sectional images.

There are three main types of OCT systems that have been introduced including the Time-Domain OCT (TD-OCT), the Spectrum-Domain OCT (SD-OCT) and the Swept-Source OCT (SSOCT). The SD-OCT and SSOCT are newer technologies as they use Fourier transform calculations in their analysis and operate at a faster rate than TD-OCT.

TD-OCT is characterized by mechanical scanning over the sample, which results in the scan rate being limited to approximately 1 kHz. In addition, due to the limitation of coherence optical path difference (OPD), the signal to noise ratio (SNR) is not comparable to that of the SD-OCT system.

SS-OCT has multiple advantages such as reduced noise, better SNR and heterodyne detection ability.[2] However, the SS-OCT system is realized in 1300 nm band in most implementations where suitable laser sources exist.[3] SS-OCT also requires a tunable high-speed swept source laser which is not simple to build. For other wavelength ranges, or preferred wavelengths, SS-OCT is not applicable. For example, 1040 nm light is more suitable for retinal imaging.[4]

In our design, the SD-OCT configuration is adopted. The SD-OCT system that we developed consists of a high-speed spectrometer and a broad-band light source in order to eliminate the disadvantages observed in TD-OCT. A 1040 nm amplified spontaneous emission (ASE) source with 120 nm FWHM bandwidth is implemented.

1.2 Development of current SD-OCT

SD-OCT was first performed by A. F. Fercher in 1995,[5] as shown in Figure 1. The central wavelength for this system was at 780 nm, and the spectral bandwidth was only 3 nm. The detection component consisted of 1800 lines/mm diffraction gratings and 320×288 pixels plane scan CCD. By performing a Fast Fourier Transform (FFT), Fercher was able to obtain the depth image of the sample. Therefore, the one-dimensional depth scan was applied to corneal thickness measurement.

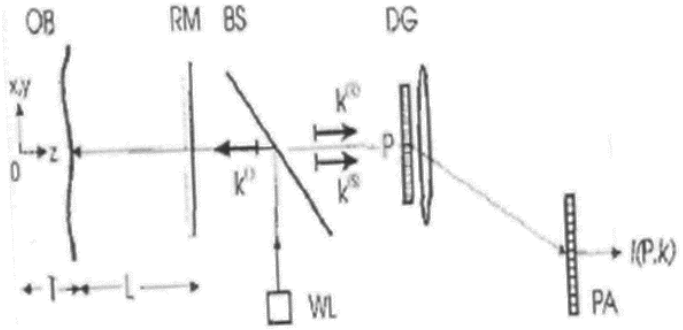

Figure 1. Schematic diagram of Fercher's OCT system

(RM stands for Reference Mirror, WL stands for white light, PA stands for pixel array)

In 1998, G. Häusler used a "Spectral Radar" system to achieve in vivo measurement of human skin surface morphology; additionally, he quantitatively verified that skin samples containing melanomas backscatter at a higher intensity than normal skin samples.[6] The system consisted of a super luminescent diode (SLD), which was characterized by a central wavelength of 840 nm, a FWHM spectral bandwidth of 20 nm, and an output power of 1.7 mW. Moreover, the system's A-scan rate was around 10 Hz and the axial resolution was measured to be 35 µm. The dynamic range could reach up to 79 dB.

In 2002, M. Wojtkowski applied the SD-OCT system to image the human retina for the first time.[7] This system consisted of a source with central wavelength of 810 nm, a FWHM spectral bandwidth of 20 nm, and an output power of 2 mW. The detection arm consisted of 1800 lines diffraction gratings and 16-bit plane scan CCD. The lateral and axial resolutions were measured to be 30 µm and 15 µm, respectively. Furthermore, the A-scan rate was 50 Hz and the dynamic range was 67 dB.

The ultra-high resolution SD-OCT developed next. Degeneration and regeneration of photoreceptors in the adult zebrafish retina have been studied by Weber et al. at an axial resolution of 3.2 µm in 2012.[8]

1.3. Structure of this report

We will first discuss the design, mechanism and methodology of the OCT system. In section 1.1, we have briefly outlined the differences between Time-Domain Optical

Coherence Tomography (TD-OCT), Spectral-Domain Optical Coherence Tomography (SD-OCT) and Swept-Source Optical Coherence Tomography (SS-OCT). Additionally, we have discussed the reasons as to why SD-OCT was chosen as the method for imaging in our system. In later chapters, the imaging contrast mechanism will be discussed in detail with calculations and derivations of important parameters.

In addition, the optical setup and a LabVIEW-based acquisition, detection and signal processing software is designed and implemented. The optical setup is fully calculated and carefully aligned with kinematic mounts and translation stages. The signal processing procedure for acquiring 2-D data sets will be studied. Additionally, an algorithm performed to increase the signal-to-noise (SNR) ratio is discussed.

Furthermore, imaging and optimization are performed during this research, and are shown in the analysis of botanic and biological tissue. In addition, the optimization for the spectrum and measurement, as well as the actual data (ex. axial resolution, image depth, etc.) are also discussed.

Chapter 2 SD-OCT Mechanisms and Calculations

2.1 SD-OCT principles

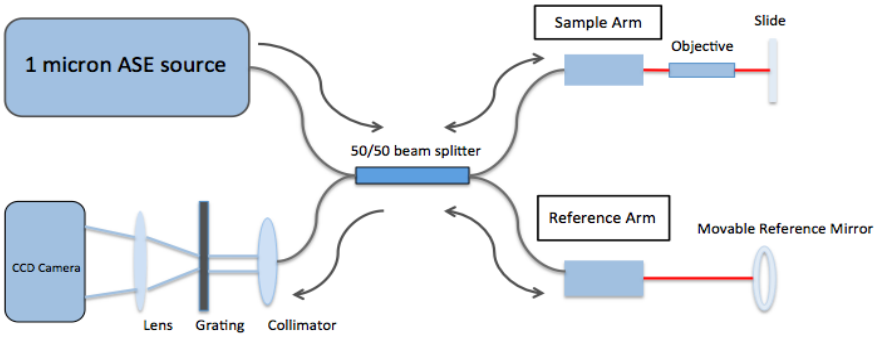

Figure 2. SD-OCT configuration

From Figure 2, we can see the SD-OCT system's configuration. SD-OCT system is based on the interferometry of the sample arm and the reference arm beam. The signal is directed into the 2 x 2 coupler and then subsequently analyzed by the OCT spectrometer. The spectrometer consists of a collimator, a transparent or reflective grating, a focusing lens, and the CCD camera. We have also added an attenuating filter in order to prevent reaching the saturation level of the CCD. The line scan CCD will acquire the A-scan data and then the computer can convert the signal by Fast Fourier Transform to develop a depth B-scan image. We will describe the data acquisition methods in Chapter 3.

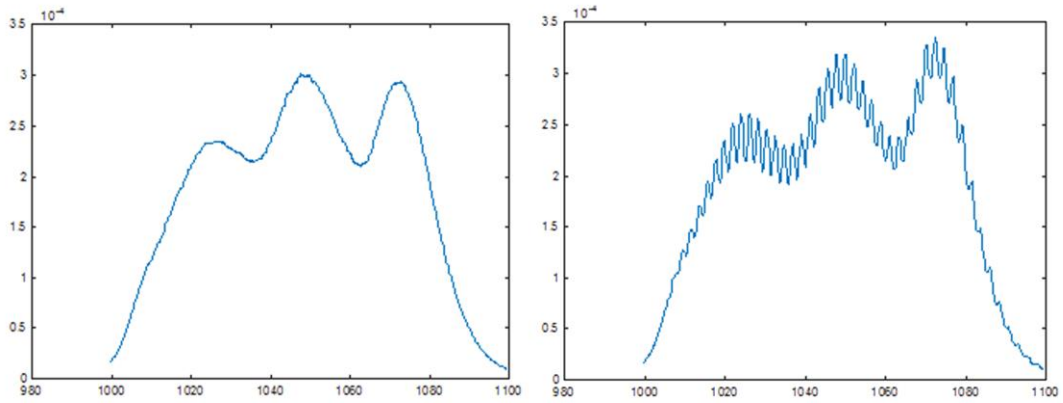

Figure 3. Laser spectrum and typical interferogram of SD-OCT

Figure 3 provides the ASE optical spectrum and a typical interferogram analyzed by an optical spectrum analyzer (OSA). The ASE source we use is centered at ~1040 nm as 1040 nm is superior at biological and ophthalmological imaging. In order to analyze

specific samples, it is essential to understand the basic math governing the imaging formation.

SD-OCT, as well as TD-OCT, has two working arms: the source and the detection arms. From the source arm, we have the incident light electric field:

Equation 1

$$E_i = S(k,w)e^{-(wt-kz)}$$

Assuming the sample is made from multiple layers, and that reflection is discrete, we have:

Equation 2

$$r_S(z_S) = \sum_{n=1}^{N} r_{Sn}\delta(z_S - z_{Sn})$$

The following equation describes the electric field of the light reflected from the sample arm:

Equation 3

$$E_S = \frac{E_i}{\sqrt{2}}\left[r_S(z_S) \otimes e^{i2kz_S}\right] = \frac{E_i}{\sqrt{2}}\sum_{n=1}^{N} r_{Sn}e^{2ikz_{Sn}}$$

This equation represents the electric field of the light reflected from the reference arm:

Equation 4

$$E_R = \frac{E_i}{\sqrt{2}}r_R e^{i2kz_R}$$

Set z=0 at the coupler, and the detector's current could be calculated as:

Equation 5

$$I_D(k,\ w) = \frac{\rho}{2} < |E_R + E_S|^2 >$$

$$= \frac{\rho}{2} < \left|\frac{S(k,w)}{\sqrt{2}}r_R e^{i(2kz_R - wt)} + \frac{S(k,w)}{\sqrt{2}}\sum_{n=1}^{N} r_{Sn}e^{i(2kz_{Sn} - wt)}\right|^2 >$$

Eliminate the w term,

Equation 6

$$I_D = \frac{\rho}{4}[S(k)(R_R + R_{S1} + R_{S2} + R_{S3} + \cdots)] +$$

$$\frac{\rho}{4}[S(k)\sum_{n=1}^{N}\sqrt{R_R R_{Sn}}(e^{i2k(z_R - z_{Sn})} + e^{-i2k(z_R - z_{Sn})})] +$$

$$\frac{\rho}{4}[S(k)\sum_{n\neq m=1}^{N}\sqrt{R_{Sn}R_{Sm}}(e^{i2k(z_{Sn} - z_{Sm})} + e^{-i2k(z_{Sn} - z_{Sm})})]$$

In this equation, there are three terms contributed to the total intensity signal: the DC term, the cross-correlation terms (CC terms) and the auto-correlation terms (AC terms).

These terms are all important in any OCT system, as every OCT system consists of these terms and each term contributes to a different signal shape. The DC term is derived from the sample reflectivity and reference reflectivity. The CC terms are generated by the sample optical path difference (OPD), which is defined by the accumulation of the interference of the sample and reference signals. Additionally, the AC terms are generated because of the accumulation of the interference of the different sample optical paths.

As the I_D is dependent on k, it is necessary to perform the Fourier transform to get the depth signal. For an arbitrary cosine function, we get the following:

$$\cos(kz_0) \overset{FT}{\Leftrightarrow} \frac{1}{2}[\delta(z+z_0)+\delta(z-z_0)]$$

After applying Fourier Transform on I_D, we will get:

Equation 7

$$I_D = \frac{\rho}{8}[\gamma(k)(R_R + R_{S1} + R_{S2} + R_{S3} + \cdots)] +$$

$$\frac{\rho}{4}\{\gamma(k) \otimes \sum_{n=1}^{N} \sqrt{R_R R_{Sn}}\, \delta[z \pm 2(z_R - z_{Sn})]\} +$$

$$\frac{\rho}{4}\{\gamma(k) \otimes \sum_{n \neq m=1}^{N} \sqrt{R_{Sn} R_{Sm}}\, \delta[z \pm 2(z_{Sn} - z_{Sm})]\}$$

Simplify the equation,

Equation 8

$$I_D = \frac{\rho}{8}[\gamma(k)(R_R + R_{S1} + R_{S2} + R_{S3} + \cdots)] +$$

$$\frac{\rho}{4}\sum_{n=1}^{N} \sqrt{R_R R_{Sn}}\, \{\gamma[2(z_R - z_{Sn})] + \gamma[-2(z_R - z_{Sn})]\} +$$

$$\frac{\rho}{4}\{\sum_{n \neq m=1}^{N} \sqrt{R_{Sn} R_{Sm}}\, \{\gamma[2(z_R - z_{Sn})] + \gamma[-2(z_R - z_{Sn})]\}$$

This is the calculation of intensity in depth of the SD-OCT system. The $R_R + R_{S1} + R_{S2} + R_{S3} + \cdots$ terms are DC terms. The $\sqrt{R_R R_{Sn}}$ terms represent the interference of the reference and sample and they are related to the cross-correlation terms. Since the R_{Sn} is relatively low compared to the reference reflectivity, a large R_R is necessary in order to obtain the accurate coherence image. Moreover, the two terms within a single CC term are symmetric and only half of the image needs to be shown after FFT. The $\sqrt{R_{Sn} R_{Sm}}$ terms are related to auto-correlation terms and they are relatively small when compared to the other two terms.

The results from Equation 8 for the example of discrete sample reflectors can be seen in Figure 4 and Figure 5. Figure 4 shows the illustration of an A-scan signal. We can see that the $S(k)$ is referred to as the source envelope and that the signal reflects cosine fringes. These fringes represent the interference of the sample and reference signals. Additionally, from the FFT of the raw A-scan data shown in Figure 5 (which refers to the intensity A-scan data), the different terms are able to be distinguished by FFT. The cross-correlation terms are discrete and reflect the reflected signals from the different depths of the sample. The B-scan image can be analyzed by merging multiple A-scan data by moving the Z/F stage.

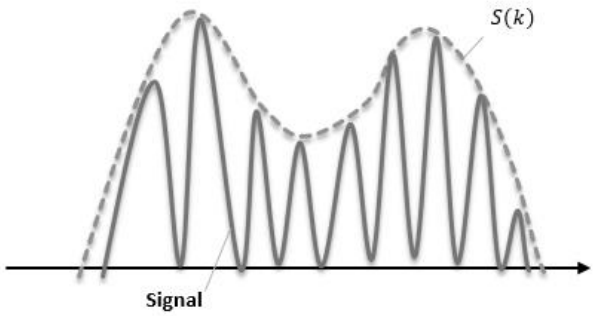

Figure 4. Illustration of A-scan sample

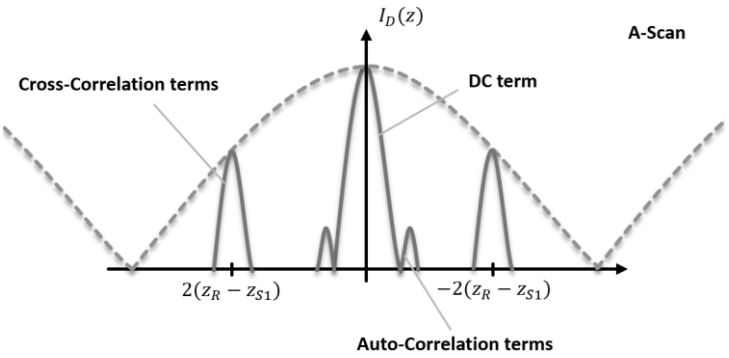

Figure 5. Illustration of an A-scan resulting from Fourier transforming

Furthermore, for multiple reflectors, the cross-correlation components in k space are superposition of fringes.[9] The super-positional cosine fringes will contribute to different peaks (distinguished with different depth difference). The analysis of spectrum may later be discussed through signal processing in Chapter 3.

In this paper, the A-scan refers to the coherence signal in the lateral direction. As opposed to in TD-OCT systems, the axial coherence signal is not needed to obtain the B-scan data in SD-OCT.

2.2 Noise in the SD-OCT system

From Equation 8, the sample information obtained by the Fourier transform is not only accompanied with the sample image, but also with correlated noise samples from the DC and AC terms. The AC and DC terms are located in the vicinity of zero optical path location, and the AC terms are related to the intensity of the sample. For highly scattering samples such as biological tissue, the autocorrelation terms are relative weak. $-z_{Sn}$ and z_{Sn} positions are symmetric and close with respect to the zero optical path. As it can be observed, the autocorrelation and DC noises reduce the final OCT image SNR and contrast. The SNR will be detailed discussed in section 2.3.3.

To minimize the autocorrelation noise of the OCT system, we apply the method of subtracting the DC term from reference. This method will be introduced in the signal processing section of Chapter 3.

2.3 SD-OCT system performance

2.3.1 Resolution

Axial resolution is related to the coherence length of the ASE source. For a central wavelength of $1040\,nm$ and $\Delta\lambda = 120\,nm$ (in our experimental setup), the axial resolution can be calculated as:

Equation 9

$$\delta z = \frac{2\ln 2}{\pi}\frac{\lambda_0^2}{\Delta\lambda} = 7.9546\,\mu m$$

Like in confocal microscopy, the lateral resolution of a SD-OCT system is defined as the sample arm focusing conditions as determined by the Rayleigh spot size and as limited by the diffraction limit restrictions. The following equation can be used to calculate the lateral resolution of our system:

$$\Delta x = \frac{4\lambda_0}{\pi}\frac{f_{obj}}{d}$$

In this equation, d is the laser spot diameter at the objective lens. For lateral resolution (x-axis), our objective lens uses a 45.06 mm focal length and 10 mm diameter (5 mm beam diameter) Carl Zeiss lens. Thus, the lateral resolution can be calculated as:

Equation 10

$$\Delta x = \frac{4\lambda_0}{\pi}\frac{f_{obj}}{d} = 11.933\,\mu m$$

Furthermore, the depth of focus (the distance at which the OCT system can see through the sample) is:

Equation 11

$$DOF = 2z_R = \frac{\pi \Delta x^2}{2\lambda_0} = 0.215\, mm$$

z_R is defined as the Rayleigh range. For different focusing lens, the beam profile can be seen in Figure 6. The use of a high NA objective lens means that the x-axis resolution can be improved – however, the resulting trade-off is that the DOF would be reduced. The greater distance away from the focus would correlate to a lesser resolution. In Figure 6, a high NA objective lens would result in less DOF that reduces the resolution outside of the depth of focus area.

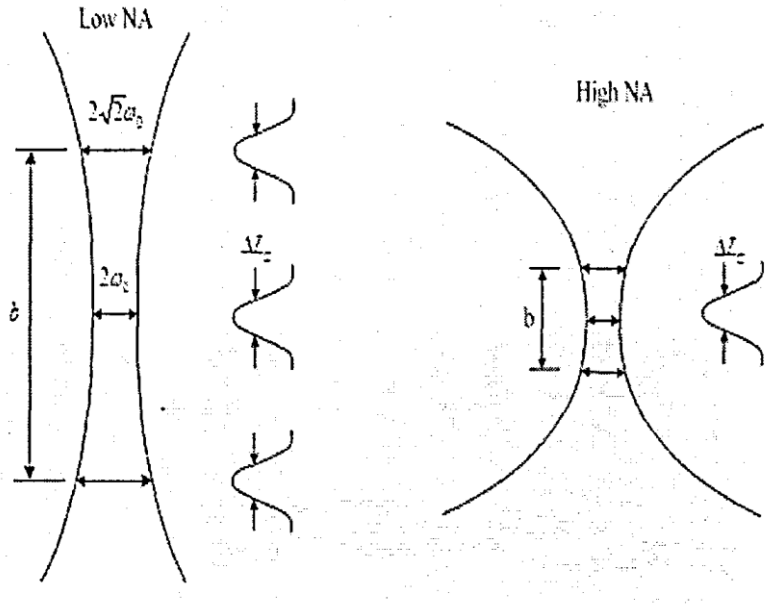

Figure 6. Low NA and high NA Rayleigh range comparison

2.3.2 Image depth

In the previous section, we discussed the depth of focus; in this section, we would like to describe the maximum image depths of our OCT system.

In SD-OCT, the imaging depth relies on the light source wavelength and power, absorption, and scattering properties of the sample. For cosine fringes with terms of $\cos(2kz)$, the frequency of k can be expressed as:

Equation 12

$$f_k = \frac{2z}{2\pi} = \frac{z}{\pi}$$

By taking the differential *k* ($k = \frac{2\pi}{\lambda}$), we can get:

$$dk = \frac{2\pi}{\lambda^2} d\lambda$$

Thus, the sampling frequency at k space would be:

Equation 13

$$F_k = \frac{1}{\delta k} = \frac{{\lambda_0}^2}{2\pi\delta\lambda}$$

The maximum of sampling at k space would be $F_k/2$, so that:

$$\frac{z_{max}}{\pi} \times n = \frac{{\lambda_0}^2}{4\pi\delta\lambda}$$

In this equation, n represents the index of the medium. The maximum image depth can be calculated as:

Equation 14

$$z_{max} = \frac{1}{4n}\frac{{\lambda_0}^2}{\delta\lambda}$$

For our SD-OCT system with $\delta\lambda = \frac{120}{1000} = 0.12\,nm$, And $n = 1.5$ for glass (for example), the image depth is $1.5\,mm$, which is similar to the depth of focus, and indicates the depth of penetration within the sample. For highly dispersive samples, we can only obtain penetration of approximately 0.6 mm.

2.3.3 Signal-to-noise ratio

To obtain the signal-to-noise ratio of SD-OCT system, we are aware that both signal and noise propagate through the spectral sampling and Fourier transform processes. The spectral interferogram of the SD-OCT system assuming a single reflector without autocorrelation terms would be:

$$I_D[k_m] = \frac{\rho}{2}S_{SDOCT}[k_m]\left(R_R + R_S + 2\sqrt{R_R R_S}\cos[2k_m(z_R - z_S)]\right)$$

In a special case that single reflector is located at $z_R = z_S$, the peak value of interferometric term is:

$$i_D[z_R = z_S] = \frac{\rho}{2}\sqrt{R_R R_S}\sum_{m=1}^{M} S_{SDOCT}[k_m] = \frac{\rho}{2}\sqrt{R_R R_S}S_{SDOCT}[k_m]M$$

This M here is the number of sample reflectors, as we assumed the sample reflectors discrete continuous. Again, assuming $R_R \gg R_S$, the shot noise limit is:

$$\sigma^2_{SDOCT}[k_m] = 2qI\Delta f = e\rho S_{SDOCT}[k_m]R_R B_{SDOCT}$$

However, the noise in each spectral channel is uncorrelated. The total shot noise is thus the integration over M. In this case, we can calculate the SNR of SD-OCT system,

$$SNR_{SDOCT} = \frac{< i_D >^2_{SDOCT}}{\sigma^2_{SDOCT}} = \frac{\rho R_S S_{SDOCT}[k_m]M}{4eB_{SDOCT}}$$

For TD-OCT system, we are also able to calculate the SNR. The well-known SNR for TD-OCT is given by:

$$SNR_{TDOCT}\frac{< i_D >^2_{TDOCT}}{\sigma^2_{TDOCT}} = \frac{\rho R_S S_{SDOCT}[k_m]}{2eB_{SDOCT}}$$

Thus we are able to say that the SNR of SD-OCT system is superior compared to the SNR of a TD-OCT system in that:

$$SNR_{SDOCT} = SNR_{TDOCT}\frac{M}{2}$$

Since the SD-OCT system offers a SNR improvement by a factor of M/2, it can be understood that SD-OCT methods sample all depths in every A-scan and result in a potential SNR improvement by a factor M; the 1/2 factor comes from the positive and negative sample displacement related to reference distance, shown in Figure 5.[10]

2.4 Grating Design

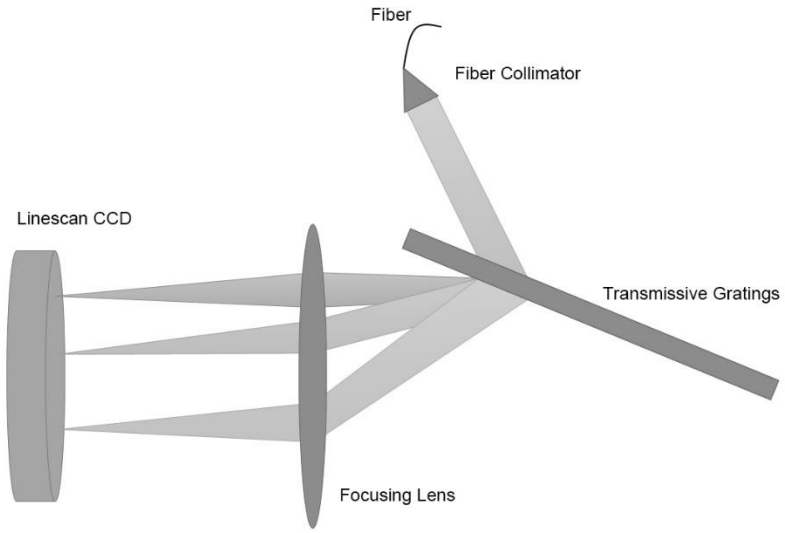

Figure 7. Grating design

The transmission grating used in our SD-OCT system has 1000 lines per millimeter . The blaze angle is 31 degrees. The CCD array is equipped with 25 μm pitch per pixel and a 1024 pixels linear array.

In chapter 2.3.2, we discussed the imaging depth of this system. In this grating design, the first constraint would be the detection array, or specifically the CCD line pixel size. The spectrum width of 120 nm must be fully captured by the CCD array so that the spectrum resolution is $\delta\lambda = 0.12\,nm$.

The second restriction would be the resolution of the grating. To be clear, a significant number of grooves must be illuminated. This depends on both the beam diameter and the density of the gratings as well as the wavelength of the light source. For N grooves,

Equation 15

$$\frac{\lambda}{\delta\lambda} = mN$$

The majority of gratings use the dispersion order of m=1. The λ here should match the largest wavelength at 1100 nm. Thus, N should be at least 9167. For density of

1000 lines/mm gratings, the beam diameter should be 9.17 mm. However, after the collimator, the beam is only 5 mm in diameter. Therefore, it is imperative to add a lens to expand the light beam to 9.17mm.

The third constraint is the diffraction gratings equation,

Equation 16

$$d(\sin\theta_i + \sin\theta_d) = m\lambda$$

After applying $\theta_i = 31°$, m=1, d=1/1000 mm, $\lambda_1 = 980\,nm$, and $\lambda_2 = 1100\,nm$ into the equation, we received the maximum and minimum diffraction angle θ_d values of 0.6248 and 0.4836, respectively.

Thus, we used OpticStudio Zemax 15 in designing the focusing lens and CCD camera. We used a 50 mm focusing lens from Thorlabs for our spectrometer. In addition, we need to see the footprint of the beam on CCD array. Figure 8 shows the layout of beam profile in Zemax.

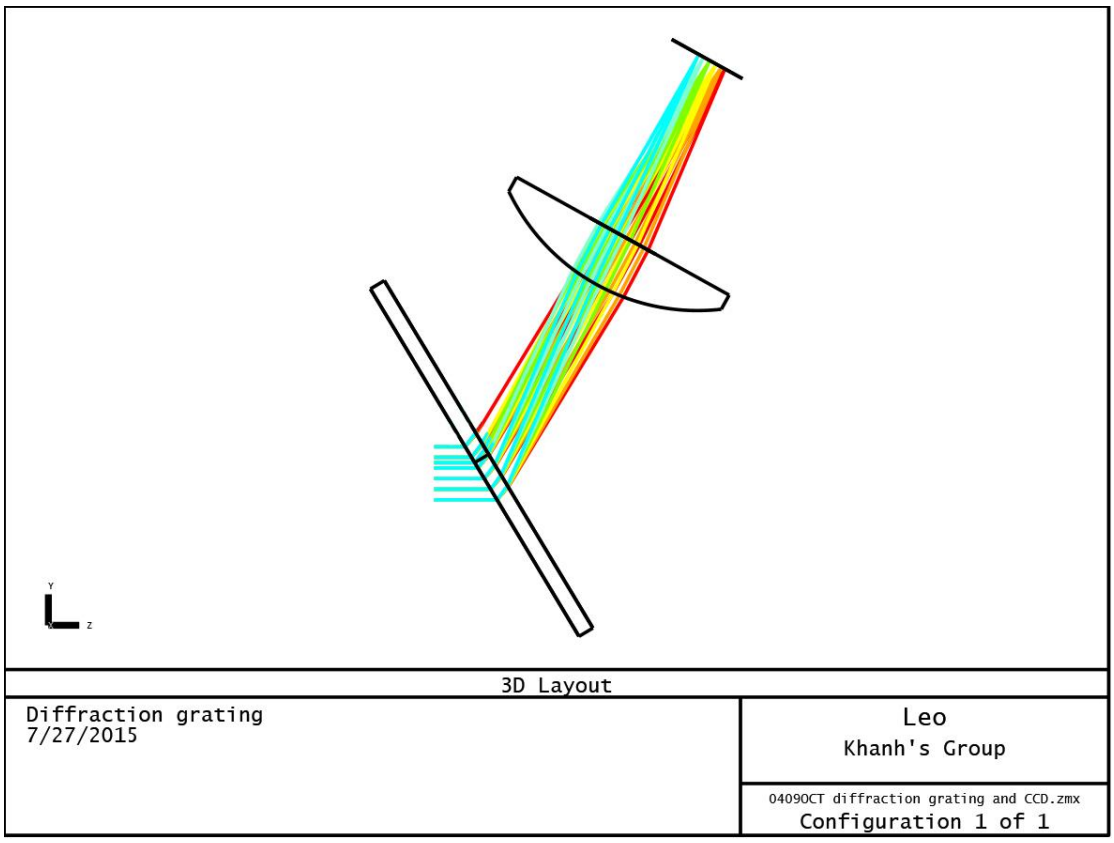

Figure 8. OCT spectrometer design by Zemax

Next, we used the optimizing option to try and get a better alignment and spot diagram. We calculated the distance from the gratings to lens to be 25.218 mm, and a focusing distance from the lens to the CCD camera to be 24.145 mm. Figure 9 shows the focusing beam on the CCD array. The spots are linear and fit for the linear CCD array.

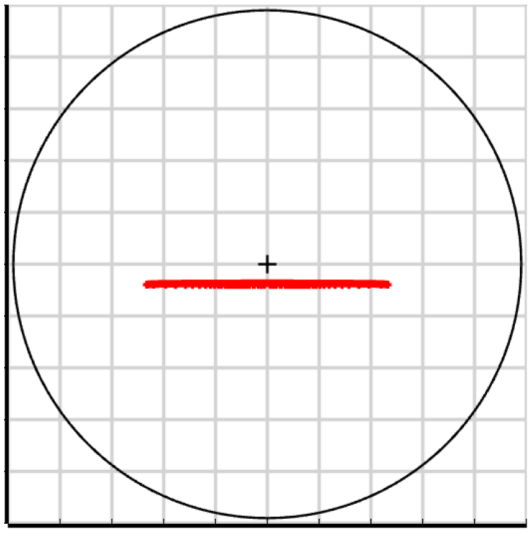

Figure 9. Footprint of the focusing beam

By adjusting the height of CCD camera, we are able to capture all the signals from OCT system and perform signal processing on a computer. The LabVIEW program carrying out this operation will be discussed in Chapter 3.

Chapter 3 SD-OCT Setup and Data Acquisition

3.1 SD-OCT System Setup

The following is a summary of the various instruments that we used in our SD-OCT system.

Table 1 Experiment preparation

Component	Specification	Comments
Line scan CCD camera	SU1024-LDH Digital Line Scan Camera from SENSORS UNLIMITED	This is a 1024-pixels high speed line scan camera. Quantum efficiency over 90% at 1040 nm. Pixel pitch at 25 micrometer. Line rate at over 46,000 lines scan per second.
Gratings	1000 lines per millimeter transmissive gratings	Diffraction angle at 31 degrees.
Objective lens	10X Carl Zeiss lens	NA=0.25, focusing length at 45.06 mm.
Laser source	1-Micron Fiber Lasers from NP Photonics	Wavelength range (FWHM) is 1.03 μm to 1.075 μm.
Z/F stage	ASI LX-4000 stage	Minimum moving distance is 0.1 μm.
Collimators	2X angled 1 micron collimator and 1X 1 micron collimator from Thorlabs	
Mirror	1X Plane mirror	
Spectrometer focusing lens	1X 60 mm reference arm focusing lens and 1X 50 mm spectrometer focusing lens from Thorlabs	
Coupler	50/50 fiber coupler	
Translation stage	2X translation stages from Thorlabs	For reference and sample arms.
Optical Power Meter (OPM)	Multi-function optical meter model 2835-C from Newport	For power detection use.
Optical Spectrum Analyzer (OSA)	Model MS9710-B from Anritsu	For spectrum analyzing.

Below is the datasheet of our system performance, based on the components we use in Table 1.

Table 2 Datasheet based on calculation of the components

Specifications	Data	Comments
Axial resolution	7.95 μm	In air.
Lateral resolution	11.93 μm	
Imaging depth	1.5 mm	Ignore dispersion for glass material.
Depth of focus	0.215 mm	
A-scan rate	46 kHz	Based on CCD measurement.
Line scan pixels	1024 $pixels$	This includes 24 dead pixels.
B-scan rate	$\sim$ 1 Hz	Based on Z/F stage, A-scan per step move.
Acquisition wavelength range	980 to 1100 nm	This value is based on spectrometer calculations.

With the components provided, we set up the SD-OCT system. Figure 10 shows our SD-OCT system with illustration. The four arms shown are source arm, sample arm, reference arm and detection arm, respectively. The four arms are connected by a fiber coupler. Sample and reference arms are aligned carefully with translation stages.

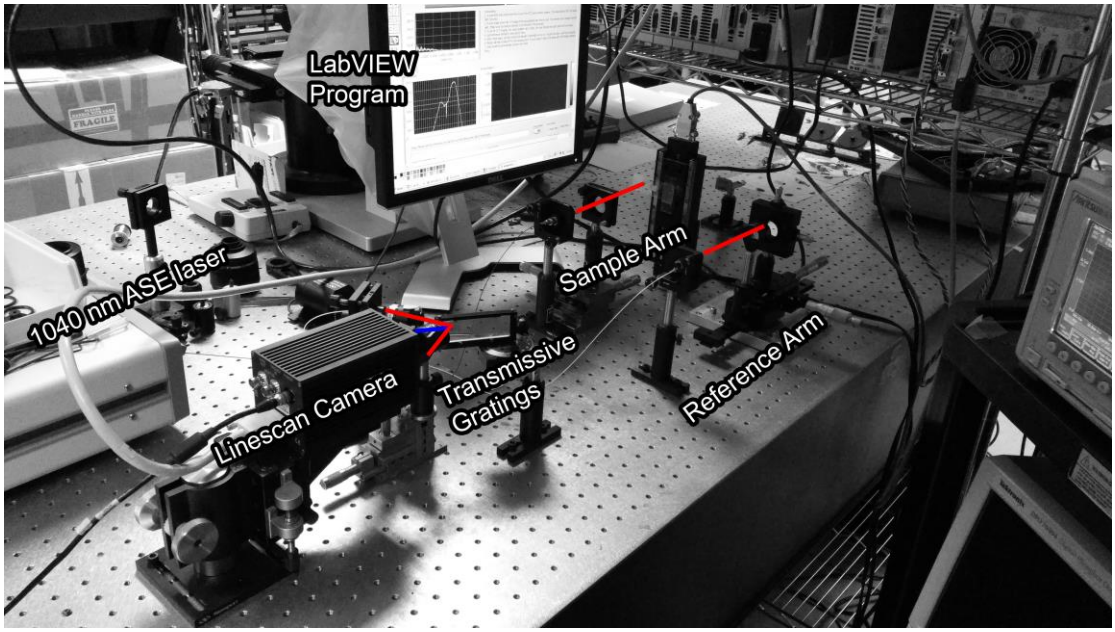

Figure 10. SD-OCT setup

The optimization and calibration of the optical setup will be discussed through later sections.

3.2 SD-OCT Data Acquisition and Signal Processing

3.2.1 Data Acquisition

In regards to data acquisition, our system uses a home-written LabVIEW software to control the line scan CCD camera to snap each line image in synchronization with the

stepping stage. The line scan CCD we use is a SU1024-LDH Linear Digital High speed InGaAs Camera from SENSORS UNLIMITED. To achieve synchronous scanning and acquisition, we used a PXI-1031 board from National Instruments to send instructions and receive data. The LabVIEW software sends an instruction to move the Z/F stage at 6 microns (half of the lateral resolution) and grab the image at the same time. This image is known as the A-scan. The B-scan image can be obtained by repeating this procedure for the determined B-scan width.

3.2.2 Signal Processing

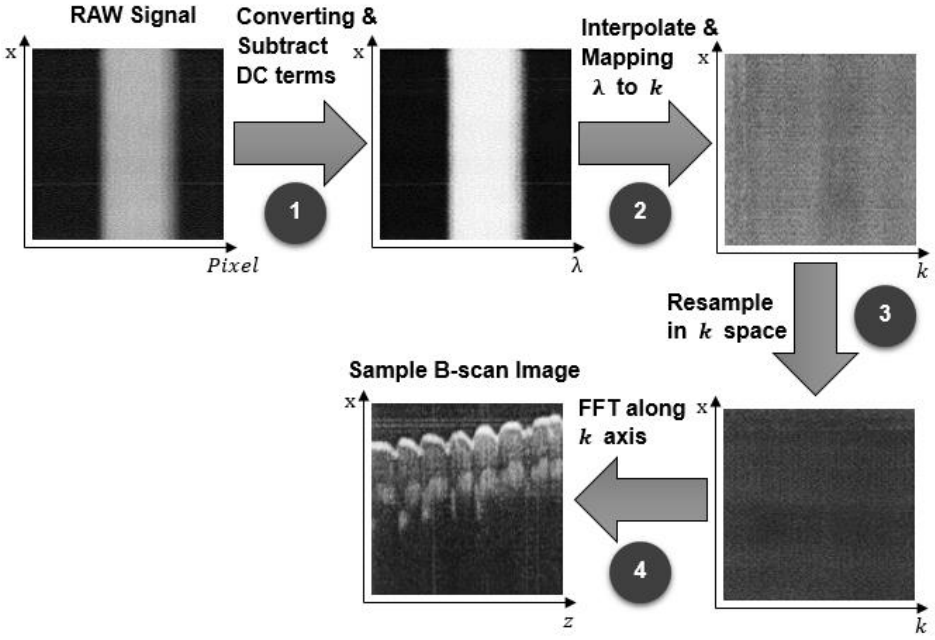

Figure 11. Signal Processing Procedure

As observed in Figure 5, this is the scheme for all signals obtained for a B-scan plane. For this system's signal processing step, each A-scan data (represented by a line in Figure 11) is obtained with respect to each pixel from the the CCD. We apply mapping from pixel number to wavelength space (refer to previous calculations). At the same time, it is necessary to subtract the DC term in order to retrieve the sample cross-correlation signal. This step is the simplest method to eliminate the artifacts in the OCT image.[11] Prior to acquiring the signal from the sample, we acquire the signals from the reference by blocking the sample beam. Next, these signals are subtracted from the interferogram formed between the reference and sample lights. This method would require such a procedure to be performed at each A-scan. In the third step, the A-scan in wavelength space is converted to a k-space signal. We use interpolation mapping to get the intensity signal versus wavenumber so that the undistorted A-scan OCT signal is retrieved. At last, after interpolation, we perform Fast Fourier Transform throughout the A-scan plane to obtain the power density versus depth profile of the sample.

3.2.3 Calibration of Depth-axis

Due to lack of two-dimensional index in LabVIEW, we have to calculate and calibrate the depth-axis to get the depth. To achieve this, we need to follow the necessary steps along with the algorithm. The pixel to wavelength conversion is based on OCT spectrometer calculations. In regards to the wavelength to wavenumber conversion, we evenly sampled the data to get k-space intensity. Next, the interpolation resampling should be performed. It is a crucial step as we can reduce the SNR and increase the on-axis resolution. We apply an interpolation factor of 1 to get the full, evenly spaced signal in k-space. After that, the Fourier transform would convert the k space data to z space and get the intensity profile A-scan. Based on the algorithm, the depth-axis then can be calibrated.

3.2.4 Software

Overall, we are able to design and test the LabVIEW program based on the algorithm described above.

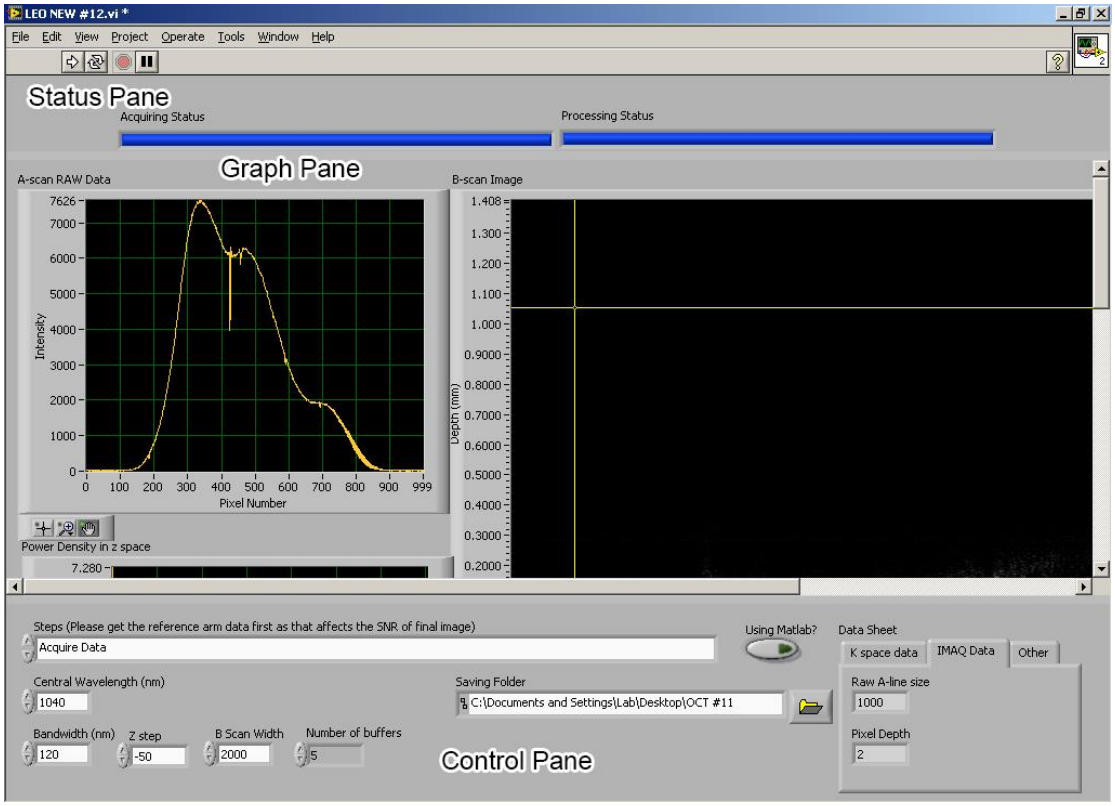

Figure 12. LabVIEW based SD-OCT system front panel

Figure 12 provides the program front panel I designed. Three panels are shown as the status panel, which indicates the progress of acquiring and processing the data; the graph panel, which shows the A-scan from camera array, depth A-scan and B-scan image; the control plane, which provides function control, adjusting the necessary experimental data and saving control.

3.3 Calibration of Sample and Reference Arms

The sample and reference signals can have a stationary interference pattern after the coupler. They must be matched in wavelength and should have a constant phase difference. Thus the reference arm length must be matched the sample arm distance. To obtain this, we use the translation stage as they can be adjusted with micrometer precision. For different samples, for instance, the onion or tissue sample on microscope cover slip, the sample arm length may vary. Thus we are to adjust both arms correspondingly. The alignment figure may be seen from Figure 13.

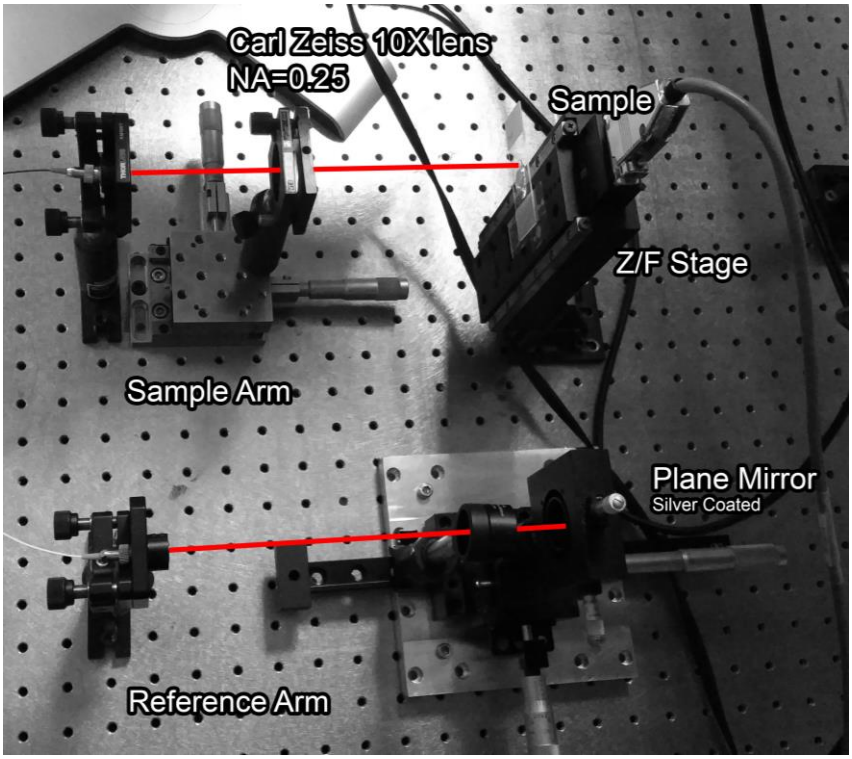

Figure 13. Sample arm and reference arm setup

The power for both arms are detected and measured respectively. The 10 mW laser source is the only source we use. The light power after the coupler is 3.805 mW according to the optical power meter (OPM). The reflected power for the aligned reference arm is ~1.29 mW. This may vary as the sample arm distance adjusted. The reflected power from sample arm is detected at ~298.0 μW for a glass cover slip and ~12.48 μW for a typical pancreatic tissue. Chapter 4 will analyze these samples and calculate the power ratio for which our SD-OCT system can detect. For our SD-OCT system, power ratio of over three thousands is achieved.

3.4 Calibration of the SD-OCT Spectrometer

The largest signal power intensity per pixel that the CCD array can recognize is over 100 and below 16000. Thus, we add a filter after the collimator at the OCT

spectrometer to reduce the amount of light reaching the CCD. The filtered light beam affects the signal-to-noise ratio a little bit.
For the CCD array, some charges in one pixel may be dispersed to adjacent pixels and cause "crosstalk"[12][13] effect. This will cause the decrease in the spectrum resolution and signal-to-noise ratio. In chapter 2 we have discussed about the spectrum resolution in grating design. One method to reduce this is to decrease the beam size at the gratings. We adjust the beam size to 5 mm without expanding the beam diameter in cost of the spectrometer resolution to 0.22 nm, but get better SNR for the spectrometer.

Another method to reduce the "crosstalk" in OCT system is to implement the non-uniform discrete Fourier transform. This algorithm is embedded to the LabVIEW program so that the interpolation in k-space is implemented together with the discrete Fourier transform. With the help of this, we have both the SNR increases and the processing time decreases.

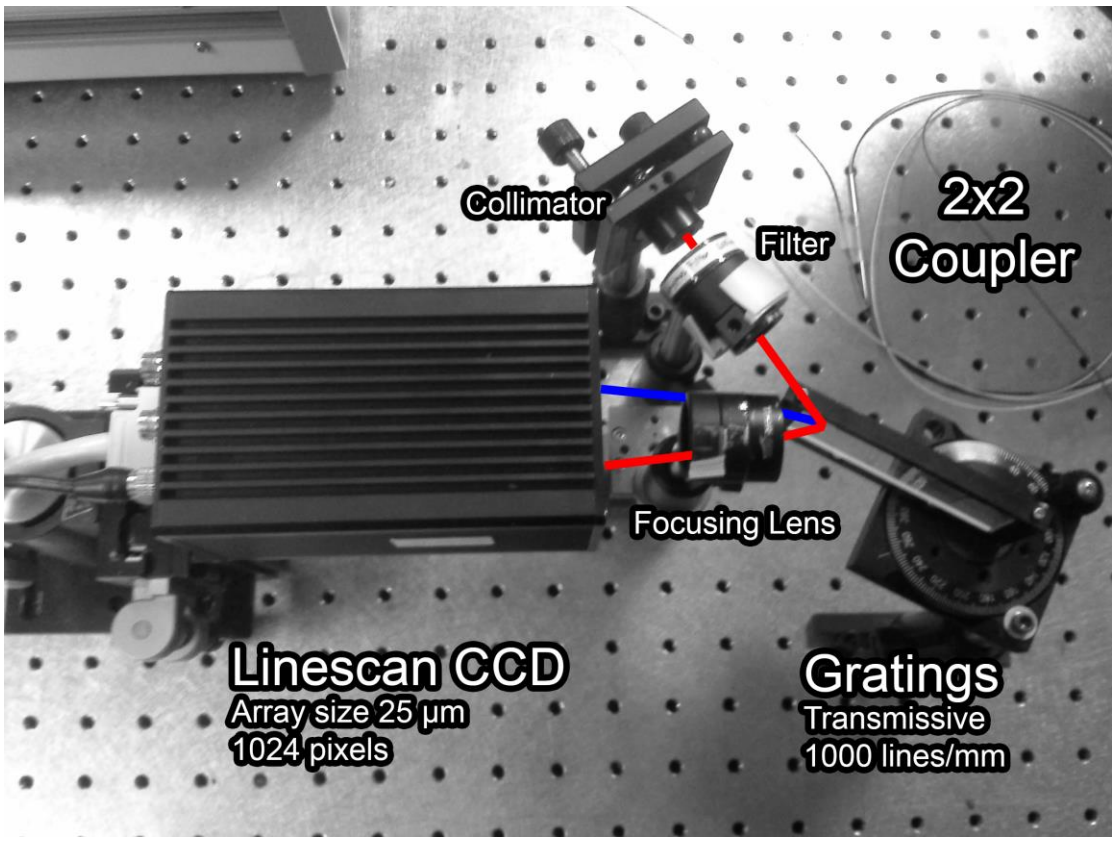

Figure 14. OCT spectrometer setup

Therefore, we are able to setup the whole OCT spectrometer part. The spectrometer setup is carefully aligned based on the calculations performed in Chapter 2.4, shown in Figure 14. The distance from the grating to the lens in this setup is approximately 2.1 centimeter, and from lens to CCD array is 4.7 centimeter. The reason for longer length form lens to CCD array is due to the refractive index in glass and focusing beam height. When moving the CCD array towards and against the lens, a noisy figure occurs.

The line beam has around 20 micrometer height. In order to make all the power to be captured by CCD array, the focusing beam need to go a little further to avoid the “crosstalk”. Thus the setup between lens and CCD array in practice is around 4.7 centimeter.

Chapter 4 SD-OCT Imaging and Optimization

4.1 Measurement of a Glass Cover Slip for calibration purpose

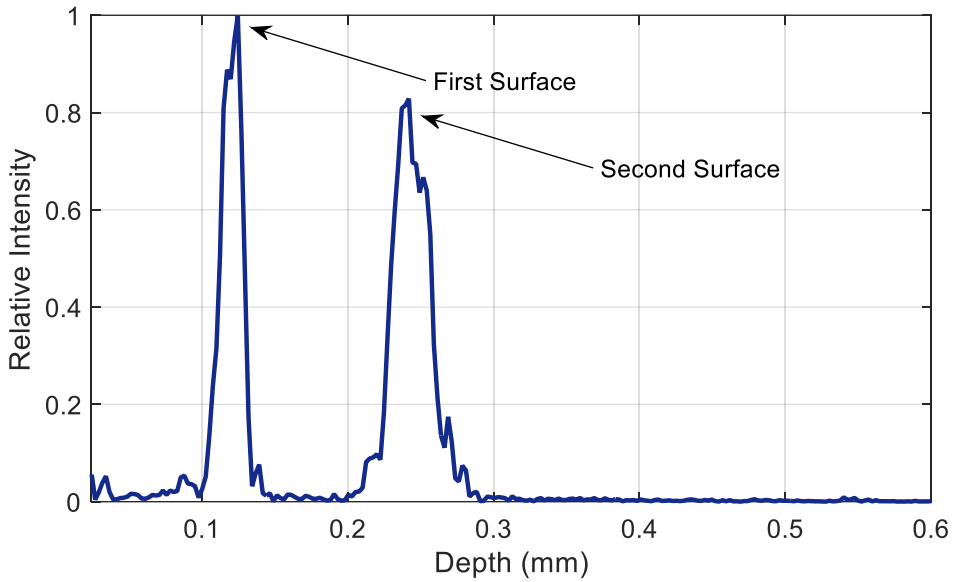

Figure 15. A-scan of a single cover slip

Figure 15 shows our SD-OCT system performance after imaging a single cover slip. The cover slip with two reflectors at a distance of approximately 0.1492 mm is distinguished. The first peak represents the light beam reflected from the first surface, and the second peak represents the back surface of the glass cover slip. The peak full-width half maximum (FWHM) is representative of our SD-OCT system resolution. The figure shows the first peak with a smaller full-width half maximum because of the depth of focus. The second peak seems noisier as the peak is far away from the center of Rayleigh range.

As the peak power also represents a relative lower intensity of 0.825, which determines that the penetration level at around 150 µm (cover slip thickness with phase of glass) had been already decreased to about 1/5 of the power. This is dependent on the depth of focus. For glass reflectors, the penetration level is around 0.8 mm, as tested in experimental data. For other materials like biological tissue or onion, the penetration level is lower compared to that of glass due to strong scattering.

For this figure, we are able to calculate the actual axial resolution. It is based on the FWHM of the first peak; the experimental axial resolution of our system can be calculated as:

Equation 17

$$Axisal\ resolution = FWHM\ (peak\ 1) = distance\ between\ \left[\frac{1}{2}\max(peak\ 1)\right]$$

$$(by\ matlab) = x_2 - x_1 = 0.0169\ mm = 16.9\ \mu m$$

For the second peak, it is wider and we also calculate the FWHM

$$FWHM\ (peak\ 2) = x_4 - x_3 = 0.0295\ mm = 29.5\ \mu m$$

The reason why FWHM of peak 2 is larger is due to the depth of focus of objective lens. As we have got 0.215 mm depth of focus from Chapter 2, the second peak which located far more beyond the center of focus thus the FWHM is wider than that of first peak. We have a test in FWHM of peak 2 when moving the peak 1 to the DC term by adjusting the reference distance. The DC term overlap the peak 1 signal and as a result, the peak 2 is closer to the center of focus of the objective. We got FWHM (peak 2)=16.3 µm. That means the two identical peak are correct according to assumption thus the reason for wider in FWHM in peak 2 is due to the high NA lens.

By testing the edge of cover slip to identify the mirror image in order to estimate the experimental lateral resolution. We see mirror images below 5.9 µm and no mirror images on and above 6.0 µm. This step is performed by the Z/F stage, which means what we can see when moving half of the lateral resolution. The mirror image stands for not seeing actual image (edge of cover slip first surface) from OCT system. Therefore, we get 12.0 µm for the experimentally measured lateral resolution.

4.2 Sample Imaging

4.2.1 Imaging of human fingernail

SD-OCT systems are superior at non-invasive imaging. We chose the human fingernail as a great sample for testing, because it is a relatively thick sample.

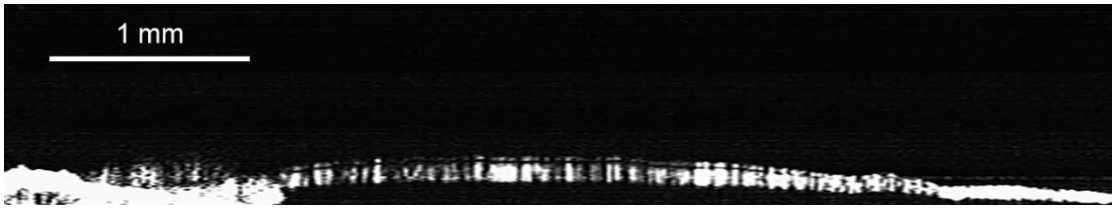

(a)

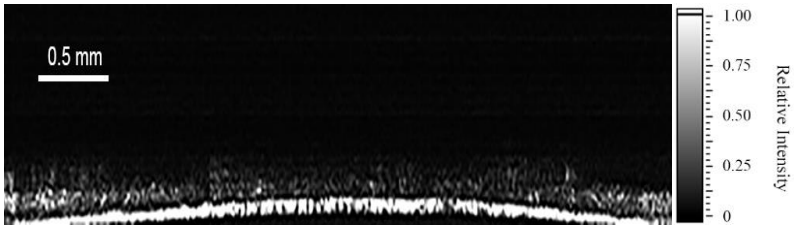

(b)

Figure 16. Human fingernail OCT image, two surfaces are clearly seen ((a) upper surface and (b) bottom surface are the nail top and (a) bottom and (b) upper are the nail bottom)

Figure 16 provides the fingernail SD-OCT image. Two of the nail surfaces are clearly seen through penetration of the laser beam. The (a) image shows the general structure of the fingernail, and (b) shows the border of fingernail (fingertip) in greater detail.

In addition, we calculated the processing time for A-scan using LabVIEW; the B-scan including 2000 A-scans elapses 16.89 seconds. Thus the processing time per A-scan is 8.445 msec.

4.2.2 Imaging of Onion

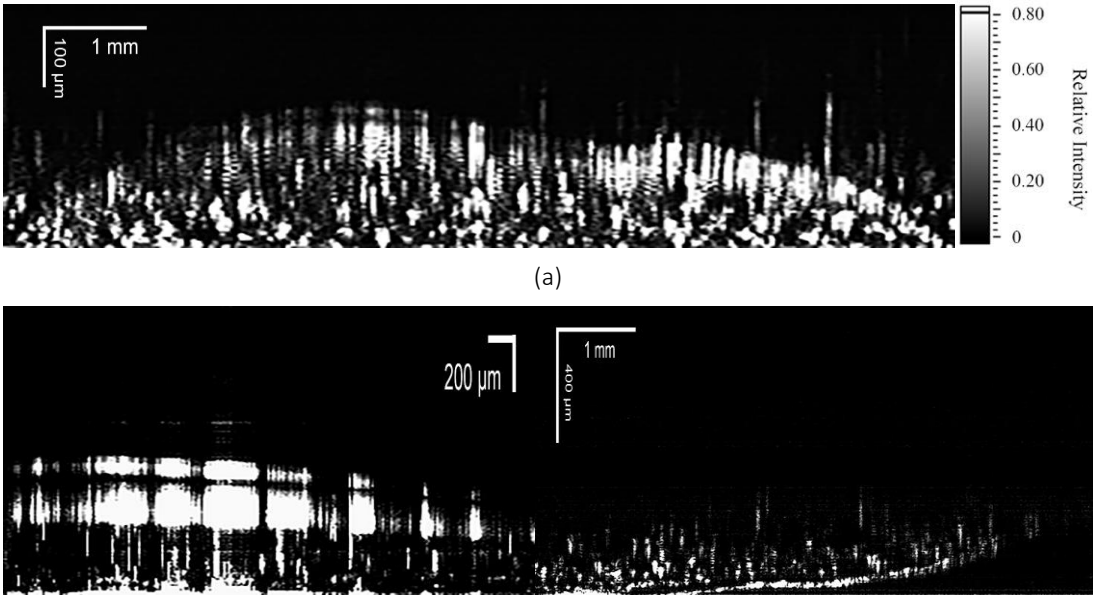

(a)

(b) (c)

Figure 17. OCT image of an onion peel ((a), total onion scanned, (b), onion peels, (c), onion cells level)

In order to determine the image depth, we also imaged some botanic tissues.

Figure 17 shows the images acquired from an onion sample that we used during OCT imaging. (a) and (b) are onions with peels. The two peels are strong in reflecting the laser beam. However, the cellular level shows greater dispersion with relatively low penetration levels for OCT. For example, (c) is the image penetration from an onion sample without peels. The cells that we can observe are around 400 micrometer in depth. The fluid in the onion is responsible for the occurrence of this effect. The water absorption coefficient is 50 times per meter at 1040 nm laser wavelength[14], which is a relatively high absorption. The high absorption of light results in lower penetration levels in tissue samples containing fluid. As a result, the hexagonal structures are not clearly seen as well.

4.2.3 Imaging of pancreas

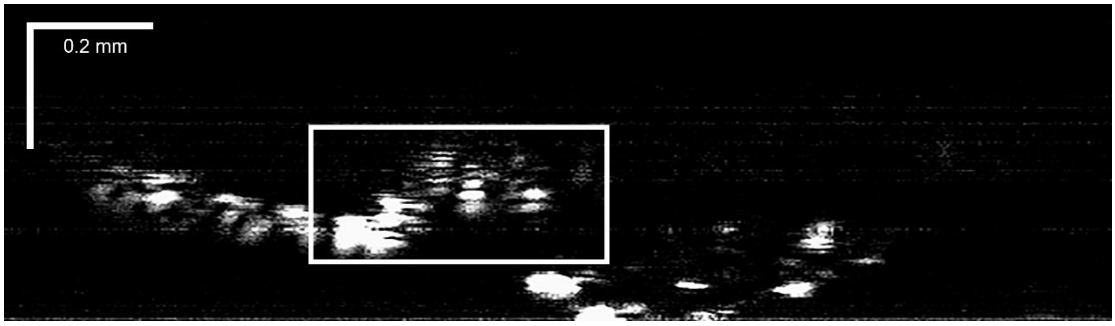

(a)

(b)

Figure 18. OCT image of pancreas ((a), pancreas structure, (b), detailed image from (a) box)

Furthermore, we also imaged a normal pancreatic tissue. The pancreatic tissue is stabilized on a microscope slip and doped chemical to prevent oxidation and resulting deterioration of the sample. The cluster of normal pancreatic cells (functional pancreatic acinus structures) are clearly seen from our OCT system. However, the much smaller islet of Langerhans cells (with a scale of 10 μm) are not able to be captured with our actual resolution of 16.7 μm. But, the (b) image shows the similar structure as islet of Langerhans.

By means of using a power meter in a pancreatic tissue test, we measure the incident power and reflected power through a single A-scan of the sample arm, to determine the power recognition of our SD-OCT system. The incident power from the collimator is about 3.805 mW. The reflected light from the pancreatic tissue sample (tested on border of pancreas with low reflected light) is 12.48 μW. That indicates that the SD-OCT can see the sample with over 3049 times from high dispersion samples. This is because the sample signal intensity with the multiplier of $\sqrt{R_R R_S}$ contributed mostly by reference signal after FFT based on SD-OCT calculations in Chapter 2.

4.3 Imaging Summary

The table below shows the experimental data for these samples.

Table 3 Experiment Datasheet

Specifications	Calculated data	Experiment Data	Comments
Axial resolution	7.95 μm	16.9 μm	Based on cover slip.
Lateral resolution	11.93 μm	12.0 μm	Based on cover slip.
Processing time		$8.445\ ms$	This time is per A-scan time elapses. Based on 2000 A-scans.
Imaging depth	$1.5\ mm$	$0.6\ mm$	For most tissues. With dispersion of material.
Reflected power ratio of sample arm		3049	Measure both the power of incident light and reflected light of a pancreatic tissue from sample arm.

The SD-OCT images are measured and captured with our system. The initial cover slip measurement verifies the setup and justifies the depth scale. The botanic tissue samples serve as a great approach in determining the actual image depth. The SD-OCT system could be a great tool to be used in clinical applications.

Chapter 5 Summary and Future Work

In summary, we have discussed the development of a SD-OCT system, as well as the important principles and characteristics of any OCT system. Research work on setting up the optical elements has been conducted. The FFT in k-space algorithm is discussed and optimized. The LabVIEW program featuring the control system and the acquisition of data is fully developed. Several SD-OCT images are taken.

The axial resolution of our OCT system is determined by the ASE light source. The coherence length in our system is calculated as 7.95 micrometer and measured as 16.9 micrometer, and is experimentally measured with a glass coverslip sample.

2-D images are obtained from our system based on the implementation of the Z/F stage used in sample arm. The A-scan rate is depend on the CCD line rate, and the processing time is 8.445 millisecond per A-scan.

Our SD-OCT system demonstrates tremendous potential in becoming a vital imaging tool for clinicians and researchers.

For future work, the most important objective should be to add a galvo-mirror system to enable 3-D imaging.

In addition, this SD-OCT system operating at a wavelength of 1040 nm has the potential to merge with other optical techniques, such as the multiphoton microscopy. In clinical use, this invention would make great contributions in the imaging and analysis of tissue.

Reference

[1] "Magnetic Resonance, a critical peer-reviewed introduction". European Magnetic Resonance Forum. Retrieved 17 November 2014.
[2] Michael A. Choma, Marinko V. Sarunic, Changhuei Yang, Joseph A. Izatt, “Sensitivity advantage of swept source and Fourier domain optical coherence tomography”, Vol. 11, No. 18 / OPTICS EXPRESS 2183
[3] Zahid Yaqoob, Jigang Wu, and Changhuei Yang, “Spectral domain optical coherence tomography: a better OCT imaging strategy”, BioTechniques 39:S6-S13 (December 2005), doi 10.2144/000112090
[4] Zhang, J., J.S. Nelson, and Z.P. Chen. 2005. Removal of a mirror image and enhancement of the signal-to-noise ratio in Fourier-domain optical coherence tomography using an electro-optic phase modulator. Opt. Lett. 30:147-149.
[5] A. F. Fercher, C. K. Hitzenberger, G. Kamp et al., “Measurement of intraocular distances by backscattering spectral interferometry,” Opt. Commun., 1995, 117: 43-48.
[6] G. Häusler and M. WLindner, “Coherence Radar” and “Spectral Radar”, -New Tools for Dermatological Diagnosis,” J. Biomed. Opt., 1998, 3: 21-31.
[7] M. Wojtkowski, R. Leitgeb, A. Kowalczyk, et al.. “In vivo human retinal imaging by Fourier domain optical coherence tomography,” J. Biomed. Opt., 2002, 7: 7457-7463.
[8] A. Weber, S. Hochmann, P. Cimalla, M. Gärtner, V. Kuscha, S. Hans, M. Geffarth, J. Kaslin, E. Koch, and M. Brand, “Characterization of light lesion paradigms and optical coherence tomography as tools to study adult retina regeneration in zebrafish,” PLoS ONE 8(11), e80483 (2013).
[9] Wolfgang Drexler and James G. Fujimoto, “Optical Coherence Tomography: Technology and Applications”, ISBN 978-3-540-77549-2
[10] M.A. Choma et al., Opt. Exp. 11(18), 2183 (2003)
[11] Ruikang K Wang and Zhenhe Ma, “A practical approach to eliminate autocorrelation artefacts for volume-rate spectral domain optical coherence tomography”, PHYSICS IN MEDICINE AND BIOLOGY, doi:10.1088/0031-9155/51/12/015.
[12] J. F. de Boer, B. Cense, B. H. Park, et al., “Improved signal-to-noise ratio in spectral-domain compared with time-domain optical coherence tomography,” Opt. Lett., 2003, 28: 2067-2069.
[13] R. Leitgeb, C. K. Hitzenberger, A. F. Fercher., “Performance of Fourier domain vs time domain optical coherence tomography,” Opt. Express, 2003, 11(8): 889-894
[14] John Bertie. "John Bertie's Download Site - Spectra". Retrieved August 8, 2012